Journal of Power Sources 195 (2010) 46–53

Contents lists available at ScienceDirect

Journal of Power Sources

journal homepage: www.elsevier.com/locate/jpowsour

Evaluation of silver as a miniature direct methanol full cell electrode

Yong Gao, Xiangxing Kong, Norman Munroe, Kinzy Jones *

Department of Mechanical and Materials Engineering, Florida International University, 10555 W. Flagler Street, Miami, FL 33174, USA

ARTICLE INFO

Article history:
Received 29 May 2009
Received in revised form 2 July 2009
Accepted 3 July 2009
Available online 5 August 2009

Keywords:
Porous silver tape
Electrode evaluation
Miniature direct methanol fuel cells
Low temperature cofired ceramics

ABSTRACT

Miniature direct methanol fuel cells (DMFCs) and direct hydrogen fuel cells are promising candidates for future polymer electrolyte membrane (PEM) based micro-power sources. Currently, most miniature DMFCs are developed using a silicon based microelectromechanical system (MEMS) technique, which requires complex and precise processing. Low temperature cofire ceramic (LTCC) technology offers an attractive alternative for a ceramics MEMS construction, allowing the integration of high density interconnect and embedded electronic components with microchannels and hermetic cavities from the meso- to the microscale. Silver is a major metallization source for LTCC, which can be fabricated in a range of configurations, from a solid hermetic layer to a porous open structure with microchannels that can easily be integrated into the structures. Silver based LTCC provides an ideal technology for the fabrication of an integrated fuel cell into a high density ceramic-based microelectronic assembly. A silver electrode was evaluated in a simulated DMFC operating environment and found to exhibit good corrosion resistance and chemical stability, essential properties for electrode systems. Potentiodynamic analysis of a catalyzed silver electrode (prepared by thermal decomposition of a Pt/Ru resinate) revealed excellent corrosion resistance under anodic and cathodic DMFC operating conditions. The Pt/Ru catalyst on the silver electrode enhanced the methanol oxidation reaction (MOR) as well as oxygen reduction reaction (ORR) as compared with similar reactions on carbon electrodes. The potential at which methanol is oxidized was lower than the silver oxidation potential, which served to protect the silver electrode. The determination of a contact angle of 30° on the silver electrode indicated wettability, which is deleterious for its application in DMFCs. Nevertheless, the results of good corrosion resistance derived from this investigation as well as the high electrical and thermal conductivities of silver all auger well for it usage as an electrode in DMFC.

1. Introduction

Direct methanol fuel cells (DMFCs) have been considered to be promising power sources for portable electronic devices such as cellular phones, personal digital assistants (PDAs), and portable computers due to their simple construction, environmentally benign nature, and projected ease of use [1–3]. Miniature DMFCs are key components in future applications integrating microsystem technologies, which will enable sensing, computing, actuation, control, and communication [4,5]. Optimized miniature DMFCs utilize small volumes and integrated structures. Current miniature fuel cells employ microelectromechanical system (MEMS) technique in their design and fabrication. However, MEMS structures are difficult to process and possess limitations in fabrication and sealing of multilayer structures [6–9]. Low temperature cofired ceramics (LTCC) is becoming more integrated as ceramic microsystems. Microsystems allow the integration of numerous components, including embedded passives, high density interconnect, high performance thermal management systems, sensors and actuators, mechanical, fluidic and optical components. The development of these systems have led to enhanced processing capabilities including enhanced properties by controlled sintering or the development of cavities and micro-electromechanical structures using fugitive inserts which are removed during firing. LTCC devices have produced meso- and macroscale channels, large volume cavities, micro-cavities, wick, valves and controlled porosity structures.

Recent work on embedded micro-heat pipes in LTCC has lead to the development of large integrated cavities (1 cm × 1 cm minimum) with cavity thicknesses varying from 25 μm to several mm. Additionally, sub-100 μm 3-D microchannels and silver structures of controlled porosity have been cofired in LTCC [10–12]. LTCC has been used by Motorola in the manufacture of a mechanically assembled DMFC [13] with the LTCC providing the mechanical structure containing microfluidic channels and cavities for fuel containment while utilizing a regular carbon-based PEM sandwiched between the electrodes. The system was mechanically assembled, loosing the packaging efficiency which a cofired, integrated LTCC structure

* Corresponding author. Tel.: +1 305 348 2345; fax: +1 305 348 1932.
E-mail address: jones@fiu.edu (K. Jones).

0378-7753/$ – see front matter © 2009 Elsevier B.V. All rights reserved.
doi:10.1016/j.jpowsour.2009.07.008

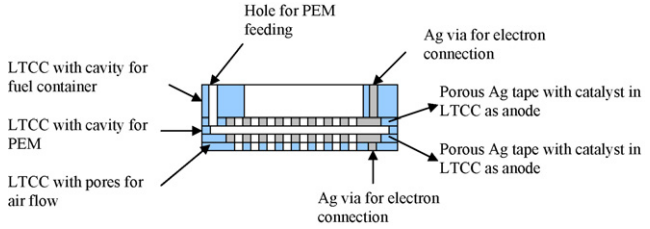

Fig. 1. A schematic illustration of an integrated LTCC-based DMFC single cell structure (not to scale).

would provide. To evaluate the possibility of a ceramic-based electrode system, a silver electrode structure was fabricated and used as the anode in a commercial carbon electrode DMFC (H-Tec Methanol Fuel Cell Junior) [14]. This demonstrated that silver metallization with a platinum/ruthenium catalyst could be developed in a cofired LTCC structure and warranted further investigation as an electrode structure DMFCs.

This paper considers the development of porous silver tape electrodes cofired into a hermetic LTCC structure with integrated cavities for fuel and micro-cavities into which the PEM is added after LTCC firing. Silver is widely used as conductive metallization in LTCC fabrication [15,16]. LTCC-based DMFC consists of the assembly of individual layers of unfired "green" LTCC tape, silver tape and fugitive materials such as carbon tape and thick film inks. The structure is laminated to develop a uniform green density, which requires all cavities/channels/voids spaces to be filled with a fugitive material such as carbon to allow uniform pressure during lamination. The LTCC structure is then fired with a multi-step profile to allow burnout of the organics and fugitive graphite until a peak of 850 °C to produce a fully sintered ceramic. Any carbon-based fugitive material burns out during sintering of the ceramic to produce cavities. Fig. 1 illustrates an integrated LTCC-based single cell. The MEA consists of anode and cathode electrodes made of porous silver tape with the catalyst added, and a LTCC cavity into which the PEM is introduced. The Silver/LTCC structure enables the fabrication of hermetic multi-fuel cells, equipped with silver-based bipolar plates.

In order to ensure good performance and extended service of the DMFC, the electrode materials must posses good electrical conductivity, chemical stability, corrosion resistance, and be capable of developing a bipolar configuration. In current DMFC, carbon (or porous carbon paper) is employed as the electrode to support the catalyst due to its high corrosion resistance and low specific density. However, the electrical conductivity and thermal conductivity of carbon are much less than those of metallic materials. Furthermore, the process for manufacturing porous carbon is very complex and time-consuming [17]. Additionally, the corrosion of carbon caused by non-uniform distribution of fuel on the anode and crossover of oxygen through the membrane separator has recently been recognized [18]. When used as a cathode, carbon is thermodynamically unstable at typical electrode operating conditions. The equilibrium potential for carbon oxidation to carbon dioxide is $-0.034\,V_{SCE}$ at 25 °C [19]. PEM fuel cell cathodes generally operate at potentials in the range of 0.26–0.66 V_{SCE}, significantly more anodic than the equilibrium potential for carbon corrosion, which could result in its degradation over time. Although thermodynamically unstable, slow kinetics allows the use of carbon in low temperature fuel-cell applications. As a result, alternative materials are being developed to replace carbon-based materials, such as conducting polymer and Ti mesh [20–22]. Such concerns with carbon electrode degradation over time are what motivated this investigation on the usage of silver as a potential electrode material.

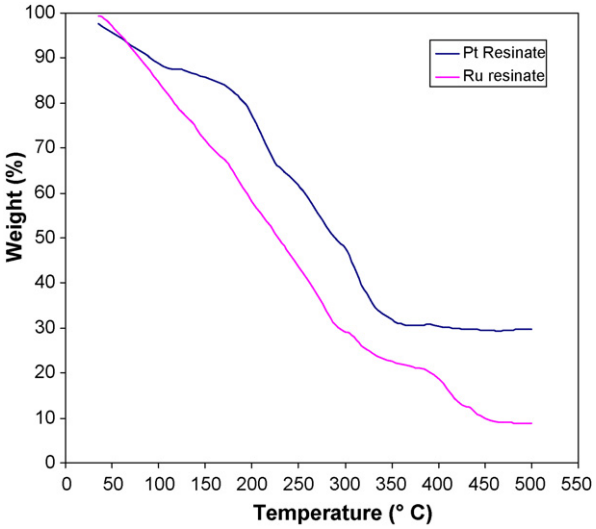

Fig. 2. The TGA curve of Pt and Ru resinate.

2. Experimental

2.1. Electrode materials and electrolytes

Silver foil (99.998% Ag, Alfa, Ward Hill, MA) was used as the electrode test material and Poco graphite sheet (Poco Graphite Inc., Decatur, Texas) was used as the carbon electrode for comparative analysis. The anode catalyst was prepared by brushing a 1:1 molar mixture of platinum resinate and ruthenium resinate (BASF, East Newark, NJ) onto the electrode (silver foil or carbon) followed by firing. The catalyst firing temperature was determined by performing a thermogravinometric analysis (Hi-Res TGA 2950, TA Instrument, New Castle, DE) on the electrode over a temperature range of 30–500 °C, with a ramp rate of 5 °C min^{-1} and a hold time of 30 min at 500 °C in air. The TGA curve (Fig. 2) indicated that Pt and Ru precipitated at 350 and 460 °C, respectively. In order to obtain the Pt–Ru alloy, a catalyst firing temperature of 500 °C for 4 h was chosen. In the case of the cathode, only platinum resinate was applied to the electrode followed by sintering under the aforementioned firing regime. Three electrolytes, 0.5 M H_2SO_4, 1 M H_2SO_4 and 0.5 M H_2SO_4 with 1 M methanol, were used in the test. All electrolytic solutions were made from analytical grade chemicals.

2.2. Electrochemical testing

A conventional three-electrode set-up in a glass corrosion cell equipped with a Luggin capillary was used in the electrochemical experiments. A platinum electrode served as the counter electrode and a saturated calomel electrode (SCE, 0.241 V vs. V_{SHE}) was used as the reference electrode. All electrochemistry measurements were conducted using a computer controlled Solartron 1287/1260 impedance system.

In order to evaluate the electrochemical behavior of silver, potentiodynamic corrosion tests were conducted to simulate the DMFC operating conditions. The anodic conditions involved the usage of 1 M methanol and 0.5 M H_2SO_4. The cathodic conditions involved the usage of 1 M H_2SO_4 with air purge. Both tests were conducted at 70 °C with a sweep rate of 1.5 mV s^{-1}. The potential range for the anodic and cathodic scan was from −0.5 V (vs. open circuit) to 1.2 V_{SCE} and from 1.2 V (vs. open circuit) to −1.0 V (vs. open circuit) respectively. The dissolved oxygen and pH were measured in each test using a water quality multimeasure sensor (PS-2169, PASCO, Roseville, CA). The solution was purged by N_2 for 30 min

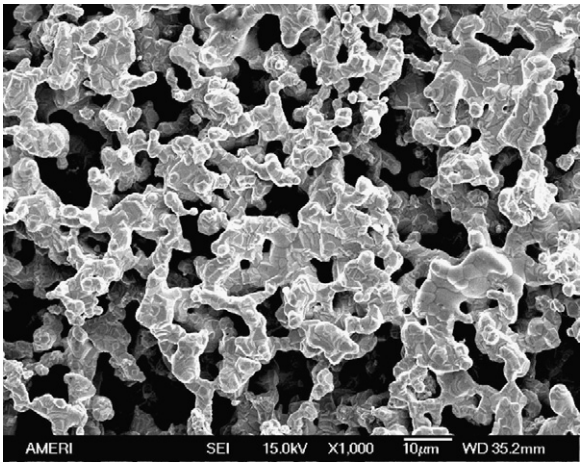

Fig. 3. The SEM photomicrograph of porous silver tape.

prior to each test and then either aerated by air or deaerated by N_2 during the test.

The corrosion resistance of silver was also assessed by potentiostaic polarization at 70 °C, by employing the abovementioned solutions but adding 2 ppm F^- [23], in an attempt to simulate the DMFC electrode environment. The applied voltages were −0.1 V_{SCE} (~0.14 V_{SHE}) for the anode and 0.6 V_{SCE} (~0.84 V_{SHE}) for the cathode, respectively.

The electrode stability was assessed by conducting cyclic voltammetry with various concentrations of H_2SO_4 and voltage scan ranges. All cyclic voltammetry tests were conducted after the electrolyte was purged with nitrogen for about 30 min to remove dissolved oxygen. Firstly, the silver electrode was scanned from 0 to 1.2 V_{SCE} at 25 °C to evaluate the effect of acid concentration. Secondly, cyclic voltammetry was conducted from 0 to 0.4 V_{SCE} for 600 cycles at a scan rate of 25 mV s^{-1} at 25 °C in 0.5 M H_2SO_4 with 1 M methanol. Additionally, methanol oxidation reaction (MOR) and oxygen reduction reaction (ORR) were evaluated by cyclic voltammetry over a scan range of 0–1.0 V_{SCE} at 20 mV s^{-1} scan rate at 60 °C. The electrolyte employed was 0.5 M H_2SO_4 with 1 M methanol for the MOR and 0.5 M H_2SO_4 for the ORR.

2.3. Tape casting

The silver electrode was fabricated by tape casting, which consisted of mixing the desired "functional" powder (ceramic, silver, carbon), dispersants, binders, plasticizers and a solvent into a slurry that was deaerated and cast on a mylar film by doctor blading. Cast thickness was adjusted by the spacing of the doctor blade. In order to produce a porous silver tape, silver powder (PM 225, Heraeus, Conshohocken, PA) was mixed with graphite powder (fugitive pore forming agent) to form the functional powder. Typically, 0.25 mm thick tapes were cast for the porous electrode, which was fired using standard LTCC firing procedures: at a heat rate of 2 °C min^{-1} to 450 °C and hold for 2 h for binder burn-out, heating 2 °C min^{-1} to 600 °C for 2 h for graphite burn-out, then heating at 2 °C min^{-1} to 850 °C for 15 min followed by a nature cooling ramp, which did not exceed 50 °C min^{-1} until cooled. The microstructure of the porous silver tape (see Fig. 3) was characterized by JEOL JSM-6330F field emission scanning electron microscope (SEM). The porosity (ε) was calculated by the following equation:

$$\varepsilon = 1 - \frac{W_A}{\rho_{real} d} \quad (1)$$

where W_A = areal weight (g cm^{-2}); ρ_{real} = solid phase density; d = thickness.

The pore size of the silver tape was measured at approximately 2–3 μm, which is consistent with the particle size of graphite powder. However, the actual porosity was determined to be 70%.

3. Results and discussion

3.1. Corrosion test

The DMFC anodic, cathodic and overall electrode reactions are shown in Eqs. (2)–(4). The potential at which MOR occurs is −0.191 V_{SCE} and ORR 0.99 V_{SCE} under standard conditions.

$$CH_3OH + H_2O \rightarrow CO_2 + 6H^+ + 6e^-, \quad E_o = -0.191\,V_{SCE} \quad (2)$$

$$3/2O_2 + 6H^+ + 6e^- \rightarrow 3H_2O, \quad E_o = 0.99\,V_{SCE} \quad (3)$$

Overall reaction

$$CH_3OH + 3/2O_2 + H_2O \rightarrow CO_2 + 3H_2O, \quad E_{cell} = 0.94\,V_{SCE} \quad (4)$$

The silver electrode was evaluated by potentiodynamic polarization analysis over the entire potential range of DMFC operating conditions. The operating conditions experienced by an electrode in a DMFC were simulated as previously mentioned in Section 2.2. Fig. 4 illustrates potentiodynamic polarization curves (anodic scan) under anode and cathode operating conditions for the silver foil and the porous silver tape. There was no significant different in

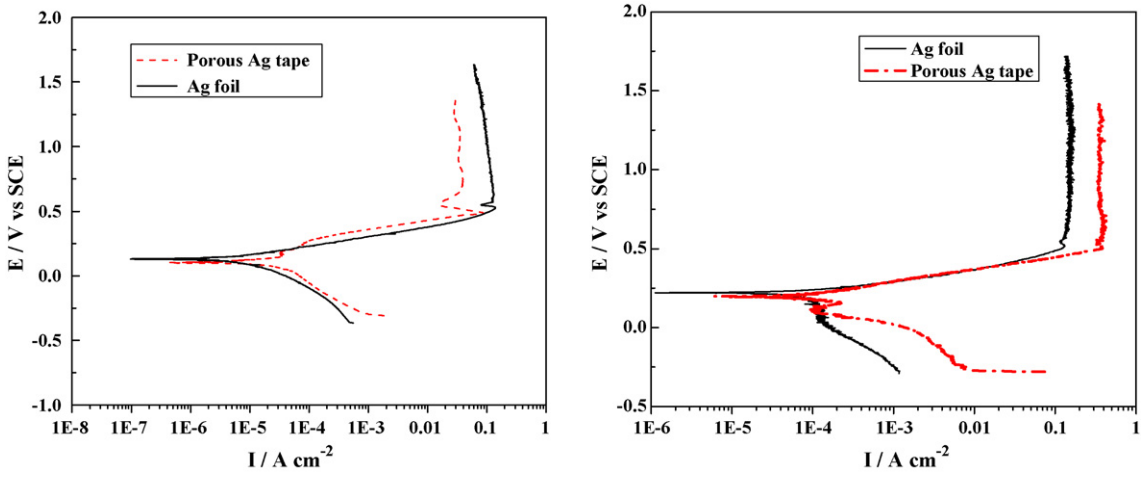

Fig. 4. Potentiodynamic polarization curves (anodic scan) of (a) silver foil and porous silver tape in 0.5 M H_2SO_4 in 1 M methanol; and (b) 1 M H_2SO_4 bubble with air at 70 °C.

Table 1
Corrosion parameters of silver foil subjected to anodic polarization under both anode and cathode operating conditions.

Corrosion parameters	Anode condition	Cathode condition
B_a (mV)	59.59	70.02
B_c (mV)	97.04	442.73
I_{corr} (μA cm^{-2})	1.94	22.74
E_{corr} (V_{SCE})	0.131	0.216
Corrosion rate (MPY)	2.578	30.166
Passivation potential (V_{SCE})	0.605	0.645
$I_{passive}$ (A cm^{-2})	0.57	0.63

Table 2
Corrosion parameters of silver foil in 1 M H_2SO_4 potentiodynamic polarization (both anodic and cathodic scan) with air purge.

Corrosion parameters	Anodic scan	Cathodic scan
B_a (mV)	70.2	19.1
B_c (mV)	442.73	133.56
I_0 (μA cm^{-2})	22.74	220
E_o (V_{SCE})	0.221	0.398
Corrosion rate (MPY)	30.166	491
Passivation potential (V_{SCE})	0.645	0.704
$I_{passive}$ (A cm^{-2})	0.63	0.08

corrosion parameters. The corrosion parameters of silver foil are summarized in Table 1.

An open circuit or rest potential of between 0.13 and 0.216 V_{SCE} was obtained for the anodic scan. At this potential the sum of the anodic and cathodic reaction rate on the electrode surface is zero and the measured current will be close to zero. According to Eq. (2), the equilibrium methanol oxidation voltage is −0.196 V_{SCE}. Therefore, silver is stable at the MOR potential because metal oxidation cannot take place at such low potential.

The cathodic polarization scan illustrated in Fig. 5 indicated an open circuit potential of 0.4 V_{SCE} for silver foil. This potential, as with the anodic scan represents the potential at which the sum of the anodic and cathodic reaction occurring on silver surface is zero. Depending on the pH and dissolved oxygen concentration in the solution, region B represents a mixed potential of oxygen reduction and H^+ reduction (hydrogen evolution or water reduction). This is apparent in the absence of a limiting current density due to limits of mass transport of O_2 to the silver surface. The potentiodynamic analysis of porous silver tape (Fig. 5(a)) resulted in the same E_{corr} and I_{corr} but some limitation of mass transport. Table 2 provides a comparison of corrosion parameters obtained from anodic and cathodic scans of silver foil under air purge. Fig. 5(b) showed the comparison of cathodic scan of silver under aerated and deaerated conditions. An increase in the open circuit potential was observed with the catalyst coated electrode. The polarization curve of deaerated silver foil showed a region that is mass transport controlled. This is to be expected, since the solution was dearated with nitrogen. A decrease in potential at region C revealed no change in the reaction rate and hence the measured current. Since this reaction is limited by how fast oxygen may diffuse (mass transport controlled) there is a limiting current density as compared to a mixed potential as previously discussed for bare silver. The measured dissolved oxygen concentration (D_{O_2}) and pH are tabulated in Table 3.

The catalyst coating on the silver electrode raised the open circuit potential as depicted in Fig. 6. Since DMFCs operate at 0.36 V_{SCE} and even lower potentials [24], it can be concluded that minimal oxidation would occur with silver electrode as well as catalyst coated electrodes. This corrosion behavior is partially attributed to the formation of the Pt–Ag alloy on the electrode surface, a phenomenon that was also observed in Pt–Ag alloy in HCl solution [25].

3.2. Electrode stability

Electrode stability in DMFCs is of paramount importance because any dissolution of metal ions may result in catalyst poisoning, and fowling of the membrane.

The evaluation of electrode corrosion resistance under DMFC operating conditions was conducted by potentiostatic measurement of the current–time relationship as shown in Fig. 7. The transient current decayed rapidly in the beginning and remained constant at -5.0×10^{-4} A due to the formation of a passive film. The negative current indicated that the electrode surface was cathodically protected, which implied no further active dissolution of the electrode under those conditions. From the relatively steady current, it can be concluded that the passive film remained very stable over time.

Potentiostatic measurement of the DMFC cathode is shown in Fig. 8, where a similar current–time relationship to that of the anode is displayed. The current in this oxidative state exhibited good stability and remained at a very low level at 0.3 μA. This current–time curve indicated that the passive film was very stable under cathodic conditions.

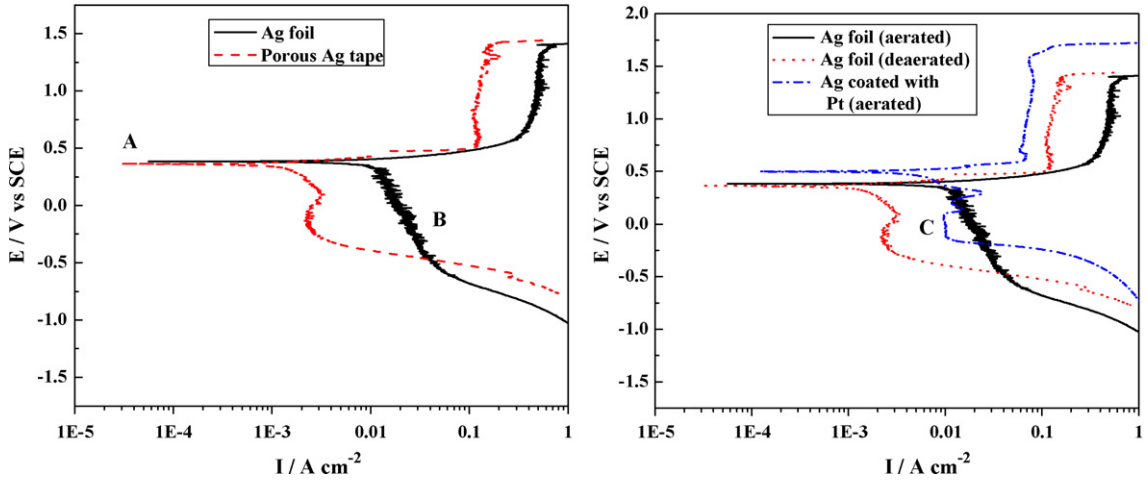

Fig. 5. Potentiodynamic polarization (cathodic scan) of (a) silver foil and porous silver tape; (b) silver foil (aerated), silver foil (deaerated), and silver foil coated with Pt in 1 M H_2SO_4 at 70 °C bubbled with air.

Table 3
Comparison dissolved oxygen concentration (D_{O_2}) and pH for cathodic scan under cathode conditions.

Samples	Conditions	Dissolved oxygen concentration (D_{O_2}) (mg L^{-1})		pH	
		Before test	After test	Before test	After test
Porous silver tape	N_2 purge 30 min; air purge during test	6.3	10.8	−2.59	−2.33
Silver foil (aerated)	N_2 purge 30 min; air purge during test	5.2	20	−0.01	0.5
Silver foil (deaerated)	N_2 purge 30 min; N_2 purge during test	10.0	16.9	−0.11	0.16

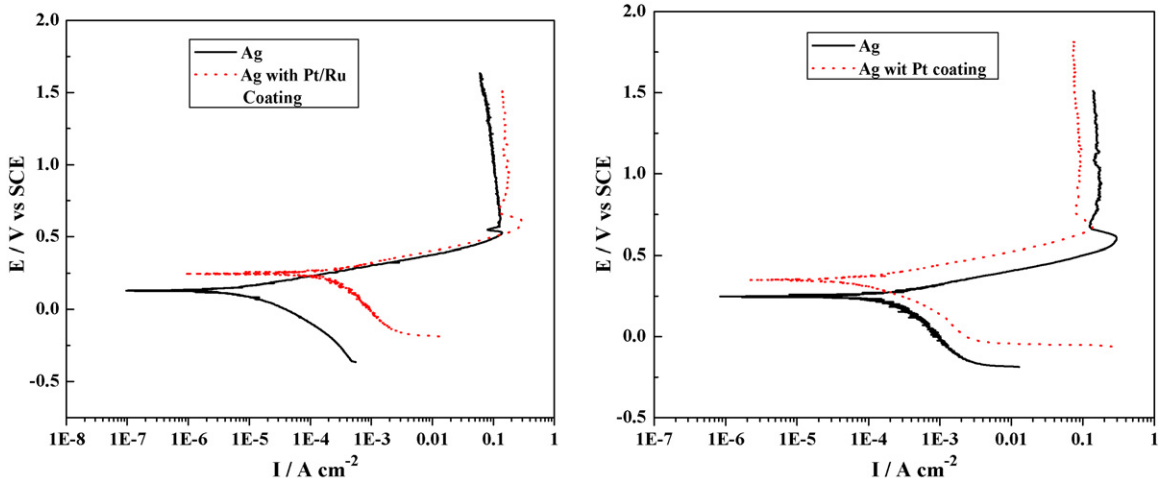

Fig. 6. Potentiodynamic polarization curves (anodic scan) of (a) silver foil coated with catalyst (Pt–Ru for anode and Pt for cathode) in 0.5 M H_2SO_4 with 1 M methanol and (b) 1 M H_2SO_4 bubble with air at 70 °C.

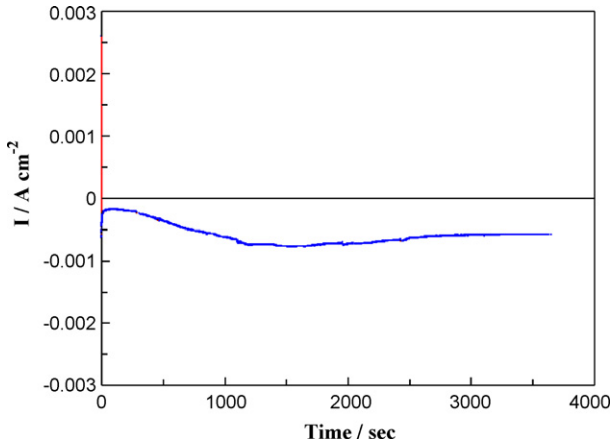

Fig. 7. Potentiostatic analysis for silver foil in 1 M methanol and 0.5 M H_2SO_4 + 2 ppm F^- at 70 °C at −0.1 V_{SCE}.

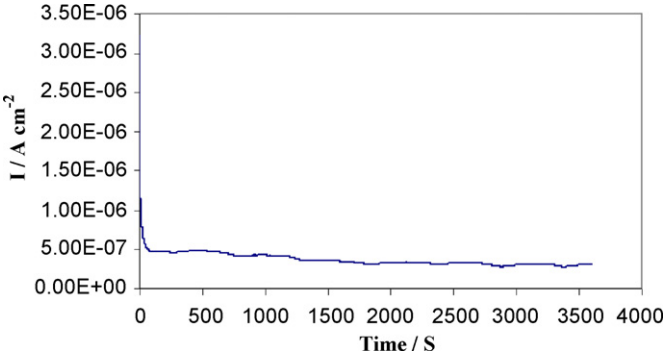

Fig. 8. Potentiostatic testing for silver foil in 1 M H_2SO_4 + 2 ppm F^- at 70 °C purged with air at 0.6 V_{SCE}.

3.3. Cyclic voltammetry

In addition to contamination of the PEM and catalytic sites [26], any electrode oxidation would result in an increase in ohmic resistance and charge transfer resistance. Cyclic voltammetry was conducted on silver in three H_2SO_4 concentrations (0.1, 0.5, and 1 M) at 25 °C as shown in Fig. 9. The onset potential of silver oxidation occurred at around 0.48 V_{SCE} with little variation as the concentration of H_2SO_4 was increased. A higher current density (larger current peak value) was obtained at higher acid concentration, which indicated greater degree of silver oxidation. It can be concluded from Fig. 8 that a change of acid environment in DMFCs has no significant effect on silver oxidation potential.

Cyclic voltammetry was conducted to test the electrode stability from 0 to 0.4 V_{SCE} at 25 °C for 600 cycles in 0.5 M H_2SO_4. The last cycle is shown in Fig. 10. There was no change in the diameter of

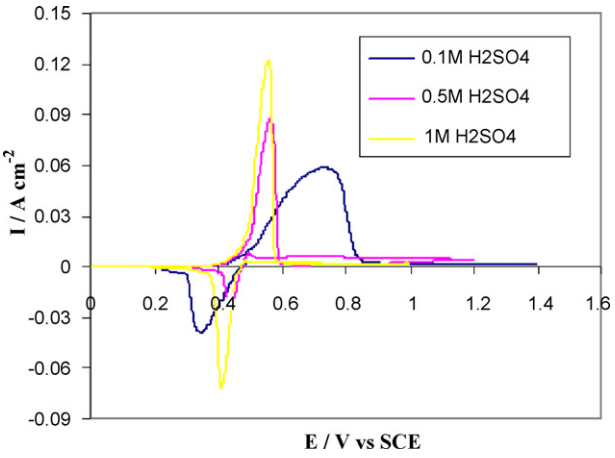

Fig. 9. Cyclic voltammetry of silver foil in different concentrations of H_2SO_4 with scan rate of 20 mV s^{-1} at 25 °C.

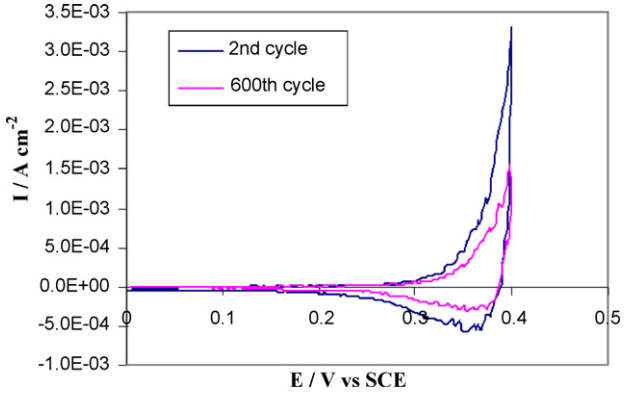

Fig. 10. Cyclic voltammetry of silver electrode after 600 cycles at scanning speed 25 mV s^{-1} at 25 °C.

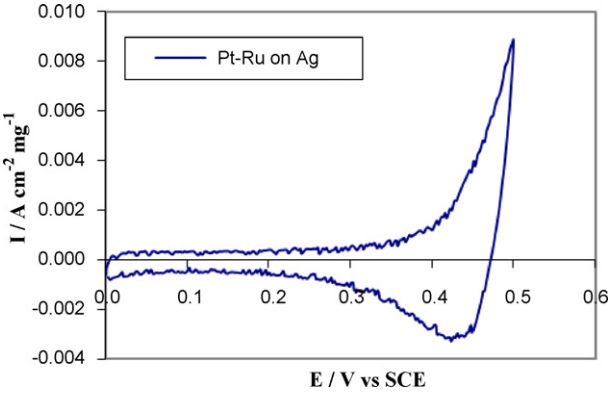

Fig. 12. Cyclic voltammetry of Pt–Ru catalyst coated on silver in 0.5 M H_2SO_4 with 1 M methanol solution at 60 °C with scan rate 20 mV s^{-1}.

the silver wire after 600 cycles under the above condition. However, the silver oxidation peak decreased after 600 cycles indicating the development of a passivating film.

Another important concern was whether the silver was oxidized before the oxidation of methanol by the catalyst. If so, it would greatly decrease the DMFC performance for two reasons: (1) oxidation of the silver electrode decreases its conductivity and (2) methanol oxidation would be limited due to less availability of catalyst. This problem depends on the onset potential of methanol oxidation by the catalyst. Fig. 11 compares the cyclic voltammograms of catalyst on silver foil and carbon. Due to the strong oxidation peak of the silver, the effect of catalyst on the carbon electrode cannot be shown on the same scale (Fig. 11(a)). Nevertheless, Fig. 11(b) shows the onset oxidation potential of methanol on a carbon electrode with catalyst at 0.32 V_{SCE}, while the onset oxidation potential of silver was 0.48 V_{SCE} as previously described in Section 3.3. It is clear that the oxidation of methanol is catalyzed by Pt–Ru before the onset of silver electrode oxidization.

It is therefore apparent in Fig. 11(a) that the peak associated with methanol oxidation is obscured by the peak for silver electrode oxidation. As can be seen in Fig. 11(b), the voltage over which methanol oxidation occurs ranged between 0.32 and 0.82 V_{SCE}, which partially overlaps the potential range over which silver is oxidized (Fig. 9). It should be noted that the peak beyond 0.8 V_{SCE} corresponded to O_2 adsorption [27].

3.4. Comparison of silver electrode and carbon electrode

ORR and MOR on a silver electrode were evaluated by cyclic voltammetry in 0.5 M H_2SO_4 and 0.5 M H_2SO_4 with 1 M methanol solutions respectively. Fig. 12 shows cyclic voltammograms of silver with Pt–Ru catalyst in 0.5 M H_2SO_4 with 1 M methanol solution over a scan range of 0–0.5 V_{SCE}. Comparing with Fig. 11(b), the MOR peak current on silver with catalyst was 3.6 times greater than that obtained on carbon. This enhancement was attributed to the Pt–Ru alloy on silver and will be analyzed in detail in another paper. Methanol oxidation on noble metal alloy has been reported elsewhere [28].

Fig. 13 compares the cyclic voltammetry for the electro-catalysis of ORR by Pt/Ag vs. Pt on carbon substrates. The peak corresponding to the mass catalytic activity of Pt/Ag (ORR) at 0.53 V_{SCE} was greater than that of Pt (ORR). There have been reports of electro-catalyzed ORR by Ag and Pt in the literature [29–32] but not as a combined catalyst. So it is reasonable to conclude that the enhanced ORR effect was primarily due to the catalytic effect of Pt–Ag that was formed on the electrode's surface. The peaks at 0.41 and 0.3 V_{SCE} in anodic and cathodic scan correspond to silver oxidation and reduction in acid solution.

3.5. Other properties

Other properties of concern include wettability and thermal conductivity of silver electrode. The presence of water results in catalyst submergence, which results in a loss of power. Electrode wettability affects cell performance, thus water should be removed immediately to avoid flooding. Surface wettability was assessed using a microscope to measure the contact angle of water on the silver electrode. Fig. 14 shows the contact angle (30°) for water on the silver surface. This value indicated that the silver electrode possessed a low surface energy, which could result in flooding of the

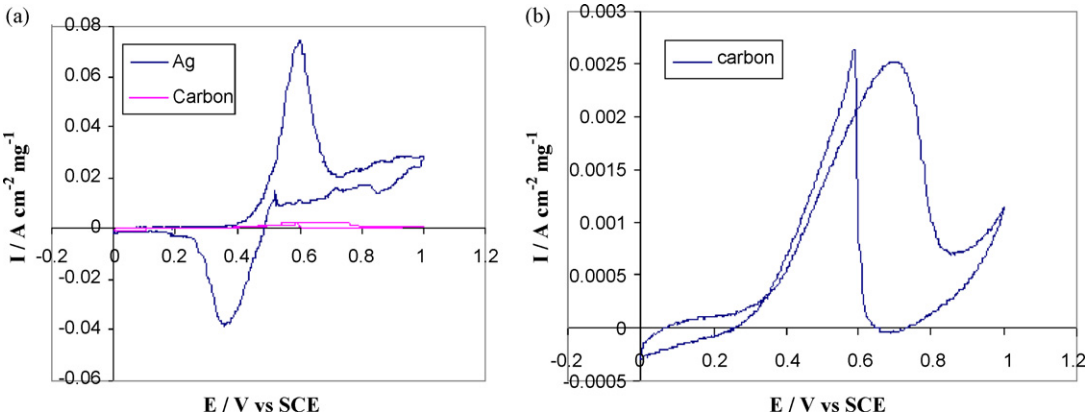

Fig. 11. The comparison of cyclic voltammetry between (a) catalyst on silver foil and (b) carbon at 60 °C in 0.5 M H_2SO_4 with 1 M methanol with the scan rate 20 mV s^{-1}.

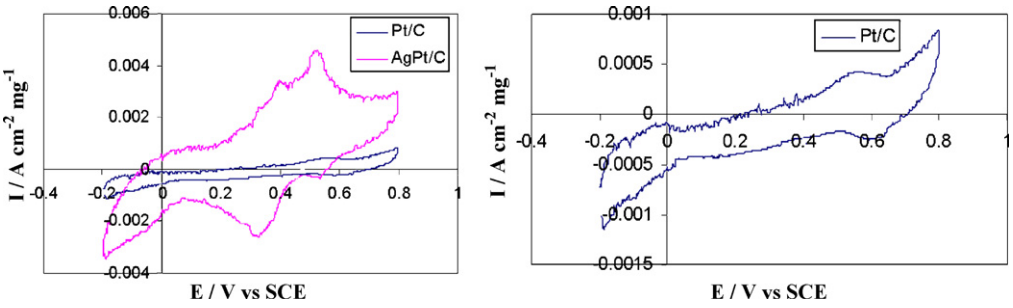

Fig. 13. Cyclic voltammetry of Pt on silver in 0.5 M H_2SO_4 with scan rate 20 mV s^{-1} at 60 °C from 0 to 0.45 V_{SCE}.

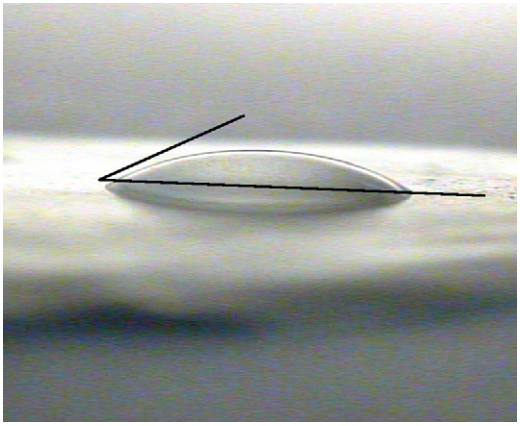

Fig. 14. Wettability of water on silver surface.

DMFC. Several approaches can be taken to enhance water removal. Firstly, a hydrophobic agent such as fluoro-octyltrichlorosilane [33], an ethanol solution of hexadecanethiol [34] or 1H,1H,2H,2H-perfluorodecyltrichlorsilane[35] could be placed on the cathodic silver surface by post-fired processing or evaporation. Secondly, laminated multilayer silver tapes with different pore size can form a wick system to expedite the removal of water.

Fuel cells can release large quantities of heat when generating electric energy during operation [36]. Less than about 30% can be expected as electricity, while the remainder is converted into heat [37]. Thermal management in DMFCs is therefore a major challenge because released thermal energy can cause discomfort for the device user. Such issues become more apparent as a growing number of miniature fuel cells become available for portable electronic power sources. The heat produced has to be dissipated, or else the accumulated heat in the system might represent a strong disadvantage for compact portable systems. High thermal conductivity materials facilitate the thermal release and are useful for thermal management in fuel cells. Since silver has the highest thermal conductivity (theoretical value 429 W m^{-1} K^{-1}) among all metals, its usage with thermal conductivity (over 100 W m^{-1} K^{-1}) is more than adequate for thermal management in DMFCs [38].

4. Conclusion

The silver electrode was evaluated by simulating aggressive environments for both anode and cathode in DMFC. Potentiodynamic test revealed the corrosion profile of silver over the entire potential range of DMFC operation. The results indicated that silver was stable under anodic conditions and was passively protected under cathodic conditions. Potentiodynamic polarization tests (cathodic scan) revealed that the cathodic reactions on the silver electrode coated with Pt was mass transport controlled (due to limits of mass transport of O_2) as compared with a mixed potential of oxygen reduction and H^+ ion reduction on a bare silver electrode. Potentiostatic analyses revealed that the silver electrode has a very low passivating current for both anodic and cathodic reactions. Cyclic voltammetry experiments demonstrated that the silver electrode was stable (no dissolution) after 600 cycles under a DMFC operation potential of 0.4 V_{SCE}. The catalyst prepared by thermal decomposition of resinate resource on the silver electrode formed Pt–Ru alloy, which increased its corrosion resistance. Experimental results indicated that MOR was more efficient on silver with catalyst under anodic conditions. Similarly, ORR reactions were also more efficient on silver with catalyst as compared with carbon. This was attributed to the formation of the alloy of Pt–Ru–Ag on the anode and Pt–Ag on the cathode. However, wettability of water on the sliver electrode indicated that it could be readily flooded. Therefore, water management would be required when silver is used in DMFCs.

References

[1] A.S. Arico, P. Creti, E. Modica, G. Monforte, V. Baglio, V. Antonucci, Electrochim. Acta 45 (2000) 4319–4328.
[2] A.S. Arico, P. Creti, P.L. Antonucci, V. Antonucci, Electrochem. Solid State Lett. 1 (1998) 66–68.
[3] K. Scott, P. Argyropoulos, K. Sundmacher, J. Electroanal. Chem. 477 (1999) 97–110.
[4] T.J. Yen, N. Fang, X. Zhang, G.Q. Lu, C.Y. Wang, Appl. Phys. Lett. 83 (2003) 4056–4058.
[5] J.H. Liu, M.K. Jeon, W.C. Choi, S.I. Woo, J. Power Sources 137 (2004) 222–227.
[6] S.C. Kelley, G.A. Deluga, W.H. Smyrl, Electrochem. Solid State Lett. 3 (2000) 407–409.
[7] G.Q. Lu, C.Y. Wang, T.J. Yen, X. Zhang, Electrochim. Acta 49 (2004) 821–828.
[8] S.-C. Yao, X.D. Tang, C.-C. Hsieh, Y. Alyousef, M. Vladimer, G.K. Fedder, C.H. Amon, Energy 31 (2006) 636–649.
[9] G.Q. Lu, C.Y. Wang, J. Power Sources 144 (2005) 141–145.
[10] M. Hrovat, D. Belavič, J. Kita, J. Cilenšek, L. Golonka, A. Dziedzic, J. Euro Ceram. Soc. 25 (2005) 3443–3450.
[11] F. Zheng, W. Wu, W.K. Jones, Int. J. Microelectron. Electron. Packaging 4 (2007) 93–98.
[12] W.K. Jones, Y. Liu, M. Gao, IEEE Trans. CPMT 36 (2003) 110–115.
[13] J. Pavio, J. Bostaph, A. Fisher, J. Hallmark, B.J. Mylan, C.G. Xie, Adv. Microelectron. 29 (2002) 1–9.
[14] N.K. Savaram, Master Thesis of Florida International University, 2006.
[15] D. Wilcox, R.F. Huang, S.X. Dai, Ceram. Trans. 97 (1999) 201–213.
[16] J.-H. Jean, Y.-C. Fang, S.X. Dai, D.L. Wilcox Sr., J. Am. Ceram. Soc. 84 (2001) 1354–1360.
[17] W. Vielstich, A. Lamm, H.A. Gasteiger, Handbook of Fuel Cells-Fundamentals, Technology and Applications, vol. 3: Fuel Cell Technology and Applications, John Wiley & Sons Ltd., New Jersey, 2003, Chapter 46, Diffusion media materials and Characterisation by Mark Mathias, Joerg Roth, Jerry Fleming and Werner Lehnert.
[18] C.A. Reiser, L. Bregoli, T.W. Patterson, J.S. Yi, J. Deliang Yang, M.L. Perry, T.D. Jarvi, Electrochem. Solid State Lett. 8 (2005) A273–A276.
[19] M. Pourbaix, Atlas of Electrochemical Equilibria in Aqueous Solutions, National Association of Corrosion Engineer, Houston, TX, 1979, p. 453.
[20] J.-H. Choi, K.-W. Park, H.-K. Lee, Y.-M. Kim, J.-S. Lee, Y.-E. Sung, Electrochim. Acta 48 (2003) 2781–2789.
[21] E.H. Yu, K. Scott, J. Electrochem. Commun. 6 (4) (2004) 361–365.
[22] Z.-G. Shao, W.-F. Lin, F. Zhu, P.A. Christensen, H. Zhang, B. Yi, J. Power Sources 160 (2006) 1003–1008.
[23] H. Wang, M.A. Sweikart, J.A. Turner, J. Power Sources 115 (2003) 243–251.

[24] F. Barbir, PEM Fuel Cells: Theory and Practice, Elsevier Academic Press, New York, 2005, p. 63.
[25] A.J. Betts, D.P. Dowling, M.L. McConnell, C. Pope, Mater. Des. 26 (2005) 217–222.
[26] E.A. Cho, U.-S. Jeon, S.-A. Hong, I.-H. Oh, S.-G. Knag, J. Power Sources 142 (2005) 177–183.
[27] D.A.J. Rand, R. Woods, J. Electroanal. Chem. 35 (1972) 209–218.
[28] D. Mott, J. Luo, P.N. Njoki, Y. Lin, L.Y. Wang, C.-J. Zhong, Catal. Today 122 (2007) 378–385.
[29] L. Demarconnay, C. Coutanceau, J.-M. Léger, Electrochim. Acta 49 (2004) 4513–4521.
[30] K. Kinoshita, J. Electrochem. Soc. 137 (1990) 845–848.
[31] H.R. Kunz, G.A. Gruver, J. Electrochem. Soc. Electrochem. Sci. Technol. 122 (1975) 1279–1287.
[32] C.-Y. Wu, P.-W. Wu, P. Lin, Y.-Y. Li, Y.-M. Lin, J. Electrochem. Soc. 154 (2007) B1059–B1062.
[33] http://www.mems-exchange.org/survey/coating_and_surface_modification/new.
[34] A Microfluidic Nanofilter, http://mrsec.wisc.edu/Edetc/nanolab/fluidics/text.html.
[35] Y. Alyousef, S.C. Yao, Microfluid Nanofluid 2 (2006) 337–344.
[36] Amir Faghri, Zhen Guo, Int. J. Heat Mass Transf. 48 (2005) 3891–3920.
[37] C.K. Dyer, J. Power Sources 106 (2002) 31–34.
[38] W. Kinzy Jones, P. Wang, Y. Liu, Proceedings of IPACK (The Pacific Rim/ASME International Electronic Packaging), Kauai, Hawaii, USA, 2001.